

**Stress Concentration Factor Determination for Various Tensile Test Specimen
Configurations by the Finite Element Method using MSC/PATRAN and
MSC/NASTRAN**

**Dr. Gregory A. Shoales, P.E.
Lt Col Scott A. Fawaz, Ph.D., P.E., USAF**

**Center for Aircraft Structural Life Extension (CAStLE)
Department of Engineering Mechanics**

**United States Air Force Academy
Colorado Springs, Colorado 80840**

February 2004

APPROVED FOR PUBLIC RELEASE; DISTRIBUTION UNLIMITED



**DEAN OF THE FACULTY
UNITED STATES AIR FORCE ACADEMY
COLORADO 80840**

USAFA TR 04-03

This technical report, Stress Concentration Factor Determination for Various Tensile Test Specimen Configurations by the Finite Element Method using MSC/PATRAN and MSC/NASTRAN, is presented as a competent treatment of the subject, worthy of publication. The United States Air Force Academy vouches for the quality of the research, without necessarily endorsing the opinions and conclusions of the authors. Therefore, the views expressed in this article are those of the authors and do not reflect the official policy or position of the United States Air Force, Department of Defense, or the US Government.

This report has been cleared for open publication and public release by the appropriate Office of Information in accordance with AFI 61-202 and USAFA FOI 190-1. This report may have unlimited distribution.



GREGORY A. SHOALES, Ph.D., PE
Senior Research Engineer,
Center for Aircraft Structural Life Extension

26 FEB 04
Date



SCOTT A. FAWAZ, Lt Col, USAF
Director, Center for Aircraft Structural Life Extension

27 Feb 04
Date



ROBERT S. FREDELL, Lt Col, USAF
Director of Faculty Research

6 May 04
Date

Abstract

Using MSC/PATRAN for pre- and post-processing of MSC/NASTRAN models, several tensile test specimen configurations were analyzed by the finite element method (FEM). Solid geometry models for each configuration were meshed using both hexagonal elements and tetrahedral elements. In all cases the mesh density was refined till the FEM solution converged. This convergence was verified both by evaluation of the solution's stability as well by various post processing tools available to the engineer within MSC/PATRAN. In each case, the ultimate goal was to determine the stress concentration factor at the specimen's net section. The sensitivity of the three dimensional stress concentration factor to specimen thickness as well as the presence of various through thickness hole sizes in the net section was also explored. In all cases, the resulting three-dimensional solution result was compared to published two dimensional elasticity solutions. While the three-dimensional FEM stress concentration solution compared favorably with the published two-dimensional values for most configurations, the same comparison for specimens with holes in the net section disagreed significantly. The disagreement between three- and two-dimensional analyses was attributed to the transition from plane stress to plain strain near thickness mid-plane. This work yielded valuable insight for the engineer as to when published handbook data will suffice and when a more detailed FEM solid model analysis is necessary. Additionally, the use of MSC/PATRAN tools for assessing model convergence is also contrasted with more the traditional technique of comparing degrees of freedom to variation in analysis result.

Contents

Abstract	i
Contents	ii
List of Figures	iii
List of Tables	iv
1. Summary	1
2. FEM Modeling and Analysis	2
2.1 ASTM E466 specimen with continuous radius between ends.....	3
2.2 ASTM E466 specimen with continuous radius between ends and net section 3/16 inch through thickness hole	9
2.3 ASTM E466 specimen with continuous radius between ends and net section 7/16 inch through thickness hole	12
2.4 Compact tensile test specimen for thicknesses of 0.125, 0.160 and 0.190 in.....	16
3. Discussion	19
4. Conclusion and Recommendations.....	21
5. References.....	22

List of Figures

Figure 1: E466 tensile test specimen with continuous radius between ends geometry	3
Figure 2: E466 specimen quarter plate model used for the analysis showing boundary conditions, loads, solid geometry and a typical mesh. Net section and gross section planes are also noted.	4
Figure 3: Typical x-component stress tensor fringe result for E466 specimen	5
Figure 4: Use of the MSC/PATRAN mesh seeding tool showing a) mesh seed applied to three curves on Solid 1 and b) the biased mesh resulting from the seeds and default global edge length.	5
Figure 5: Degrees of freedom versus maximum net section stress for various meshes.	6
Figure 6: Result A10 with difference plot option for x-component stress tensor fringe plot...	7
Figure 7: Example disabling the MSC/PATRAN averaging feature as a means of discerning model convergence in a) poorly converged model and a b) well converged model.	7
Figure 8: E466 specimen (results case A10) maximum axial stress versus through thickness (z) location at the net section outside corner (x=0 in, y=0.5 in)	8
Figure 9: Solid model geometry required for MSC/PATRAN iso-meshing of E466 specimen with a net section through thickness hole.....	9
Figure 10: Degrees of freedom versus maximum net section stress for ASTM E466 specimen with 3/16 in net section through thickness hole.....	10
Figure 11: Comparison of FEM 3-D solution with handbook [1] 2-D solution for stress tensor x component versus through thickness (z) location at the net section top of hole (x=0 in, y=0.09375 in) of E466 specimen with 3/16 in through thickness hole.	11
Figure 12: Degrees of freedom versus maximum net section stress for ASTM E466 specimen with 7/16 in net section through thickness hole.....	12
Figure 13: MSC/PATRAN contour plot of a) stress with element to element averaging disabled and b) maximum difference between all solutions for each node in the “mesh bias” model solution for E466 specimen with 7/16 in net section through thickness hole	13
Figure 14: Comparison of FEM 3-D solution with handbook [1] 2-D solution for axial stress versus through thickness (z) location at the net section top of hole (x=0 in, y=0.21875 in) in E466 specimen with 7/16 in through thickness hole.....	15
Figure 15: Plan view of compact test specimen used in CASTLE Research Center fatigue effect from exfoliation studies	16
Figure 16: Compact tensile specimen quarter plate model used for the analysis showing boundary conditions, loads and solid geometry. Net and gross section planes are noted.	16
Figure 17: MSC/PATRAN contour plot of a) stress with element to element averaging disabled and b) maximum difference between all solutions for each node in the 0.125 in thick compact test specimen model	17
Figure 18: Axial stress from 3-D FEM solution versus thickness plane for three thicknesses modeled of the compact tensile test specimen. Handbook [1] 2-D solution is also shown	19

List of Tables

Table 1: Convergence study results for E466 quarter plate model..... 4
Table 2: Summary of FEM 3-D K_{tN} results compared with 2-D handbook [1] K_{tN} 19

1. Summary

Accurate determination of stress concentration factors is critical to predicting material behavior during all manner of mechanical testing. Depending on the test goal, tensile test specimens will vary in overall dimensions, as well as geometric features. Dimensions will vary in thickness, width and test section length. Geometric features may include such things as notches, holes, blending from gripping surface to the net test section, and other variations necessary to achieve the desired test condition. Exhaustive stress concentration factor figures and tables have been published by Pilkey and Young [1, 2] which account for a wide variety of possible specimen configurations. However, many of these readily available sources of stress concentration factors consider only a two-dimensional theory of elasticity solution. When the specimen geometry is such that three-dimensional effects become more dominant, the engineer must turn to other analysis techniques such as the finite element method (FEM) to find accurate stress concentration factors. The present work not only uses FEM solid modeling to determine stress concentration factors for various specimen shapes but also serves to identify which shapes may require finite element modeling for accurate stress assessment as opposed to those for which handbook solutions will suffice. All FEM analysis work was performed with MSC/NASTRAN using MSC/PATRAN for pre- and post-processing.

An ASTM E466 specimen was the first to be analyzed [3]. While the E466 tapers down from the gross section (grip area) to the net section by a ratio of nearly 2 to 1, the blending is such that it yields a very small, 1.03, net section stress concentration factor (K_{tN}). In this case the three-dimensional FEM solid model analysis agreed precisely with the handbook result [1, pp. 86]. This specimen was then modified to explore the effect of through thickness holes at the net section. Specifically, a 3/16 in and a 7/16 in were modeled. The published K_{tN} for the ASTM E466 with 3/16 in and 7/16 in net section through holes is 2.54 and 2.20, respectively [1, pp. 256]. As is often the case with the handbook solutions, the table referenced here is not a precise match to the test specimen configuration but rather the best match available. The 3-D FEM model yielded maximum K_{tN} values for the ASTM E466 specimen with 3/16 in and 7/16 in net section through holes of 2.68 and 2.26, respectively. Therefore the 3-D K_{tN} for the ASTM E466 specimen with 3/16 in and 7/16 in net section through holes are greater than their respective 2-D handbook values by 6 and 3%.

The last specimen modeled was a compact hour glass specimen. In this case the same planer shape was modeled for three different thicknesses, namely 0.125, 0.160 and 0.190 in. In this case the handbook solution for K_{tN} of 1.13 [1, pp. 84] was in agreement with the FEM 3-D analysis for all three thickness. While there was an observable thickness effect which increased the maximum stress at the hole bore's center as the model thickness increased, the impact was negligibly different from the published value.

The engineer should consider the level of fidelity required by their analysis when using stress concentration factors provided by the tables and equations in the commonly accepted handbooks. While these offer very quick answers without the time and effort required by advanced FEM solid model analysis, they may not offer the desired accuracy. This is particularly the case for test specimens of increased thickness or complex levels of geometric detail.

2. FEM Modeling and Analysis

All tensile test specimens investigated in the present work were model using MSC/NASTRAN solid elements. Material properties used were of a “generic” aluminum with stiffness (E) of $10E6 \text{ lb/in}^2$ and Poisson’s ratio (ν) of 0.3. All specimens were loaded only in the long-axis direction with the model’s global x-axis oriented in that direction. All specimens were constant thickness with the thickness dimension oriented with the model’s z-axis. The model’s y-axis therefore describes the width dimension, perpendicular to the loading direction. The specimens investigated here vary in width from the largest width where the axial load is applied (the gross section) to the smallest width (the net section). It is at this net section where the maximum stress concentration occurs and it is the manner in which the specimen’s width dimensions transition from the gross section to the net section that influences the magnitude of the stress concentration. This stress concentration is over and above the increased stress that is present simply because of the reduced net section area. One customary way to express this is by the net section stress concentration factor (K_{tN}). K_{tN} is the ratio of the maximum net section stress (σ_{Max}) to the nominal net section stress (S_N). The σ_{Max} is due to the stress concentration caused by the geometric features of the net section. In the present work it will be determined by the FEM analysis. The S_N is simply found by dividing the axial load (P) by the net section area (A_N) where A_N is the product of net section width (w_N) and specimen thickness (t) as shown in Equation 1.

$$S_N = \frac{P}{A_N} \quad (1)$$

$$S_N = \frac{P}{w_N \cdot t} \cdot (\text{lb} / \text{in}^2)$$

Combining this calculated S_N with the σ_{Max} found in the FEM analysis, K_{tN} is found by the relationship shown in Equation 2.

$$K_{tN} = \frac{\sigma_{Max}}{S_N} \quad (2)$$

For computational simplicity, each specimen was also modeled using quarter plate symmetry such that the net section is on the $x=0$ plane. Symmetry boundary conditions are applied to the $y=0$ and $x=0$ plane. A unit stress (1 lb/in^2) is applied to the gross section (S_G) at the x-y plane. Therefore, given t , S_G and the gross section width (w_G), the applied load (P) can be expressed as shown in Equation 3.

$$P = S_G \cdot w_G \cdot t \cdot (\text{lb}) \quad (3)$$

With a constant specimen thickness and the applied 1 lb/in^2 stress, S_N is now expressed as the ratio of gross section width to net section width (w_N) as shown in Equation 4.

$$S_N = \frac{P}{w_N \cdot t} = \frac{S_G \cdot w_G \cdot t}{w_N \cdot t} = S_G \cdot \frac{w_G}{w_N} = (1 \cdot lb/in^2) \cdot \frac{w_G}{w_N} \tag{4}$$

$$S_N = \frac{w_G}{w_N} \cdot (lb/in^2)$$

Therefore given this calculated S_N and σ_{Max} found from the FEM solid model analysis, a true three-dimensional (3-D) K_{tN} is determined for each tensile specimen modeled. The following subsections describe the detailed method, assumptions, and procedures used while creating the solid model and performing FEM analysis for each of the investigated tensile test specimens. The specimen dimensions pertinent to the discussion in this section will be highlighted as Equation 4 is applied to each specimen

2.1 ASTM E466 specimen with continuous radius between ends

This ASTM specimen features a very gradual blending from the gross section width to the net section width. The aim of this design is minimize the stress concentration due to the width change while still providing a definite net section upon which to focus the test. Figure 1 shows the detailed geometry for this specimen

Thickness, T	Test Section Width, W	Notch Root Radius, R	Test Section Length, L	Test Section Area	Grip Length, L _g	Grip Width, W _g	Grip Area	W/T	Theta	h
(in.)	(in.)	(in.)	(in.)	(in ²)	(in.)	(in.)	(in ²)		(rad)	(in.)
0.250	1.00	10.00	6.00	0.250	3.000	1.921	0.480	4	0.609	0.461

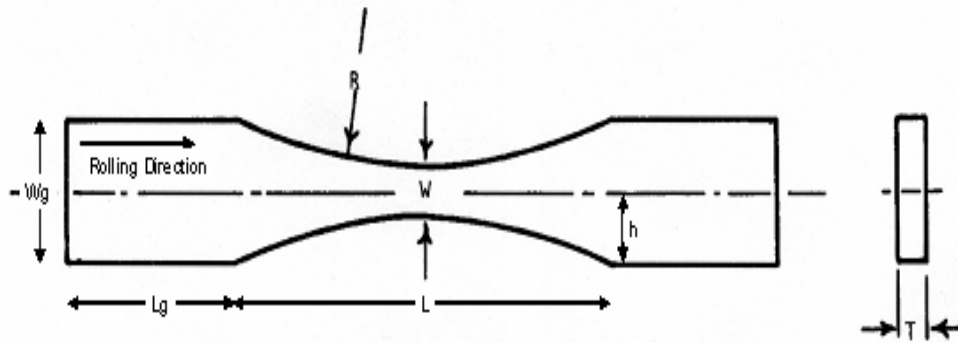


Figure 1: E466 tensile test specimen with continuous radius between ends geometry

A quarter plate solid model of the E466 specimen was defined in MSC/PATRAN as shown in Figure 2. As viewed in this figure, symmetry displacement constraints boundary conditions were imposed along the entire xz-plane at y=0 and yz-plane at x=0. A 1 lb/in² pressure was applied to the entire yz-plane at x=6 in. As the quarter plate model is viewed in Figure 2 the origin is at the lower left corner.

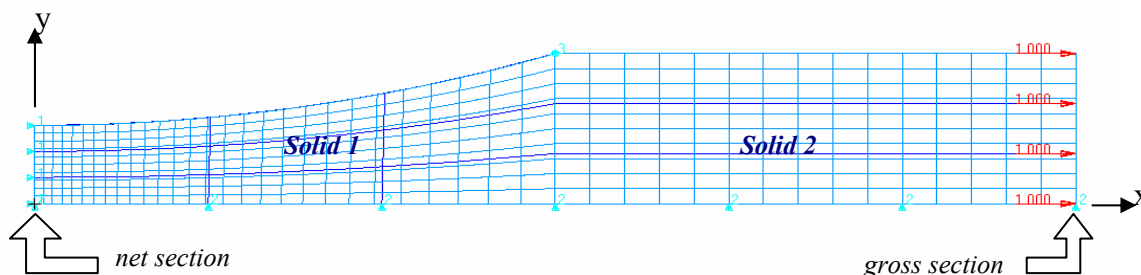


Figure 2: E466 specimen quarter plate model used for the analysis showing boundary conditions, loads, solid geometry and a typical mesh. Net section and gross section planes are also noted.

The quarter plate model was actually composed of two separate geometric solids, Solid 1 forming the portion which blends from the gross section width down to the net section width, and Solid 2 forming the constant width portion. This geometry definition was necessary in order to create what MSC/PATRAN refers to as an iso-meshable parametric solid as required by the mesh generator for hexagonal elements [4]. As they are applied to the E466 model geometry, these iso-meshable parametric solids are easily formed by extruding surfaces composed of no more than four sides through the specimen's thickness. For the initial meshing quadratic solid MSC/NASTRAN Hex 20 elements were chosen. The mesh was automatically generated by the MSC/PATRAN tool using a geometry based default element size as defined by a parameter called the global edge length (**GEL**). As the name implies, **GEL** gives the mesh generator a target element edge size to use when dividing larger solids into smaller elements. For both solids the defaults **GEL** was approximately 0.5 in. As might be expected, this produced a somewhat course mesh with 594 degrees of freedom (**DoF**) and resulted in a σ_{Max} of 1.99525 lb/in². The unusually high number of reported digits was required to illustrate the effects—many very small—discussed in this work. Additional meshes were then generated by selecting progressively smaller values for **GEL**. The maximum stress was noted for each mesh in order to judge the level of convergence. This process was then repeated for tetrahedral solid MSC/NASTRAN Tet 10 elements. Table 1 summarizes the method and result of the convergence studies.

Table 1: Convergence study results for E466 quarter plate model

Result Case	Element Type	Degrees of Freedom	σ_{Max} (lb/in ²)	GEL (in)
A1	Hex 20	594	1.99525	MSC PATTRAN default (~ 0.5)
A2	Hex 20	3,502	1.98521	0.2
A3	Hex 20	20,924	1.98461	0.1
A4	Hex 20	163,401	1.98419	0.05
A5	Hex 20	89,426	1.98419	0.05 on solid 1, default on solid 2
A6	Tet 10	929	2.00037	MSC PATTRAN default (~ 0.5)
A7	Tet 10	8,247	1.98552	0.2
A8	Tet 10	47,024	1.98481	0.1
A9	Tet 10	133,576	1.98418	0.05 on solid 1, default on solid 2
A10	Hex 20	24,242	1.98423	mesh seeding in solid 1, default in solid 2

Several key points are worth noting here. First, the Hex 20 elements seemed to approach the convergent solution with fewer elements (lower *DoF*). Next, the progression from case A4 to A5 was based on the recognition that the increased mesh density (due to the decreased *GEL*) was only necessary in the Solid 1 where, as illustrated in Figure 3, the stress concentration occurs as a result of the change in width. In the constant width Solid 2, the mesh was left at the default setting. As shown by the result, despite a 45% reduction in *DoF*, the σ_{Max} is unchanged. Therefore, if some engineering judgment is used to determine where increased mesh density is warranted, a convergent solution is obtained while still retaining a computationally economical solution. Such judgment was applied to evolve from case A8 to A9 with the Tet 10 element solutions. Here again, the same S_N results was achieved as the A4 (Hex 20) result case with $\sim 20\%$ decrease in *DoF*—this despite the previous observation that the Hex 20 elements solutions converge at lower *DoF*.

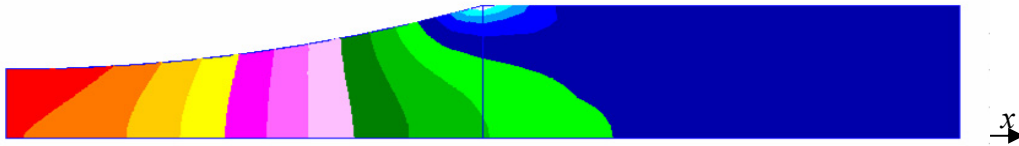


Figure 3: Typical x-component stress tensor fringe result for E466 specimen

Taking this engineering judgment to the logical conclusion and using one of the MSC/PATRAN mesh tools, result case A10 represents nearly the same level of convergence as A4 with less than 15% of the latter's *DoF*. For this result case, the MSC/PATRAN *mesh seeding* tool was used to force nodes to a desired density at the area of highest stress concentration, namely the net section. The tool was further used to keep the Hex 20 element side dimensions as uniform as possible in the net section region. Lastly, a mesh seed was applied to smoothly transition the mesh size to Solid 2 where larger elements are possible. The mesh seed is represented graphically by the yellow circles shown in Figure 4a. Once the mesh seed was imposed the MSC/PATRAN automatic mesh generator was used with default *GEL* to attain the mesh illustrated in Figure 4b.

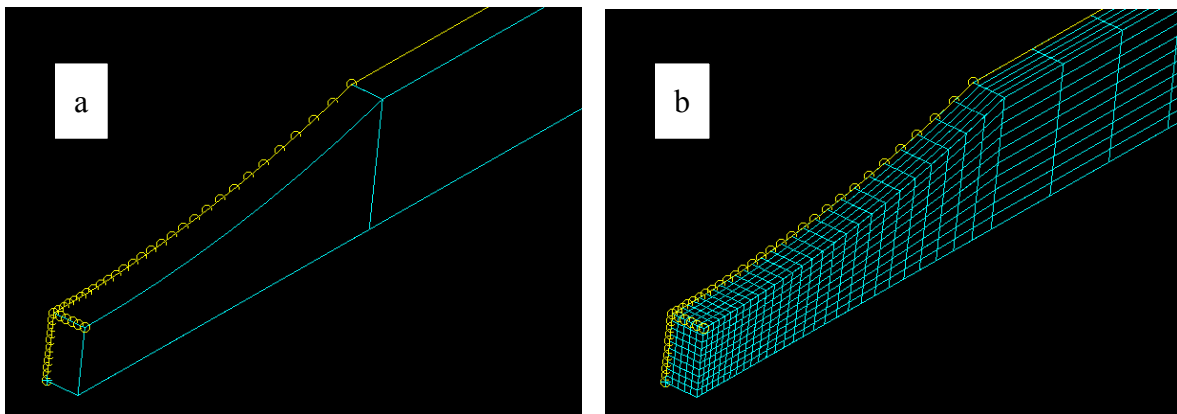


Figure 4: Use of the MSC/PATRAN mesh seeding tool showing a) mesh seed applied to three curves on Solid 1 and b) the biased mesh resulting from the seeds and default global edge length.

Figure 5 compares all the result cases graphically as a plot of DoF versus S_N and clearly illustrates both the quality and the computational economy (low DoF) of the A10 result case with the mesh biased by the mesh seeding tool.

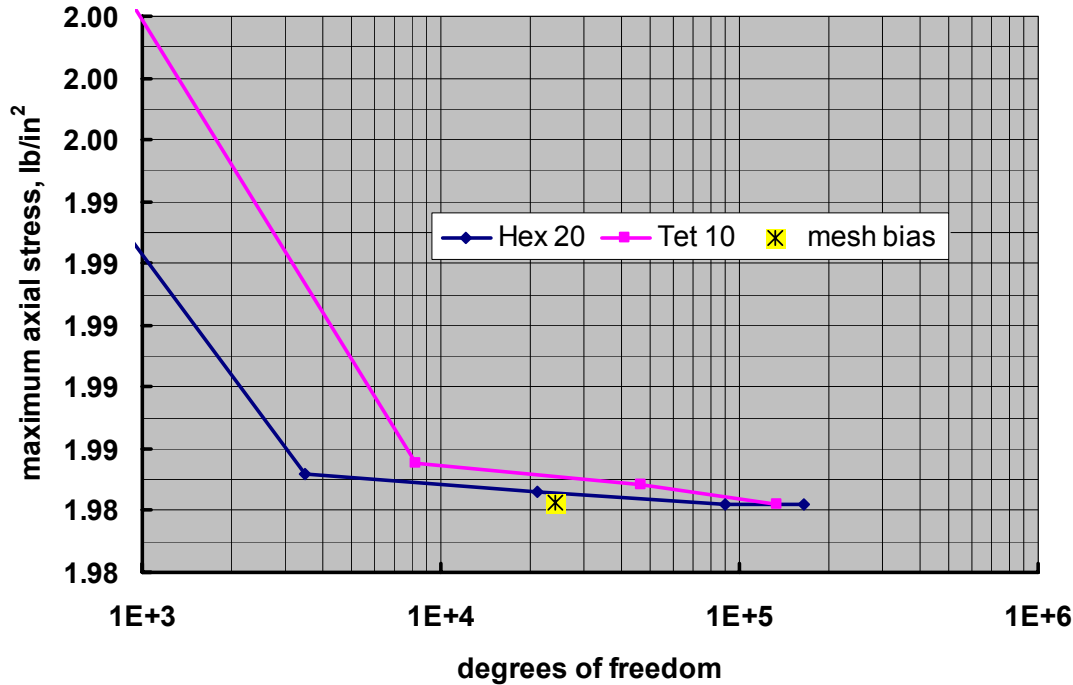


Figure 5: Degrees of freedom versus maximum net section stress for various meshes.

In addition to the more conventional convergence study just discussed, MSC/PATRAN offers a multitude of tools to judge the overall quality of solution. These graphical tools exist in the post processing section of the program under the *Results* “button.” In order for MSC/PATRAN to create fringe plots such that shown in Figure 3, the program must first deal with the fact that solutions of adjoining elements might attain different stress solutions for the nodes where they intersect one another. In a solid mesh with quadratic elements any given node may therefore have as many as 8 different solutions stemming from each of the surrounding elements. In a convergent or “well-behaved” solution such differences will be well below the level of significance in the desired of the FEM analysis [4].

The node result differences can be shown in a fringe plot by selecting “difference” as the averaging method under the MSC/PATRAN fringe plot options. This option then shows the magnitude of the absolute difference between the largest and smallest solutions at any given node. Individual nodes or regions can further be selected to focus on the convergence of any given portion of the model. Figure 6 focuses on the set section of the E466 specimen model and shows the difference plot option when employed for result case A10. As shown in this figure, the maximum difference between solutions for any given node near the net section is only 1.07E-4 which is 0.005% of the stress result for that region—arguably well below any reasonable level of significance for the FEM stress result.

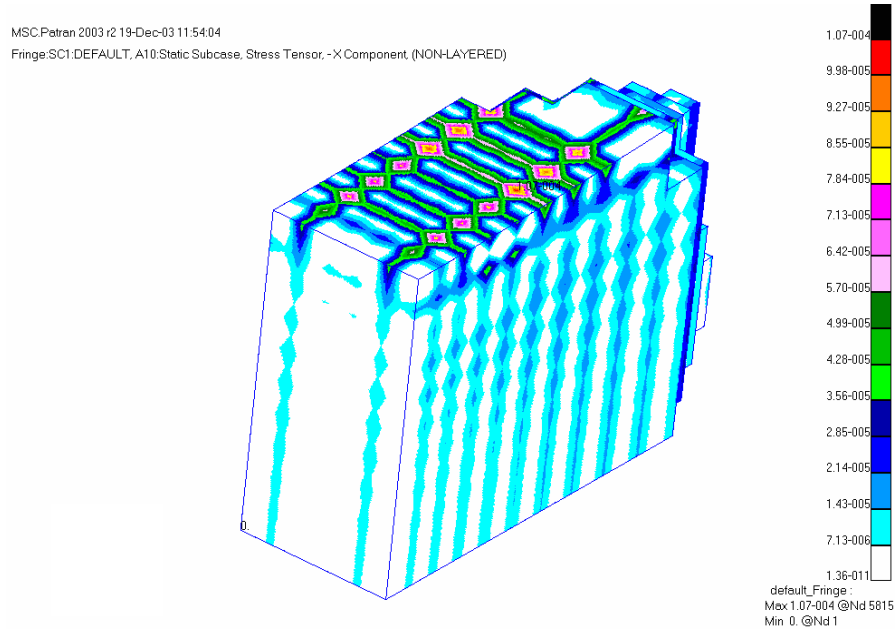


Figure 6: Result A10 with difference plot option for x-component stress tensor fringe plot

The next technique used to graphically judge model convergence was to purposely disable the feature that permits MSC/PATRAN to produce smooth contours in the fringe plots. As previously stated, one would expect a convergent solution to have little or no difference between the solutions calculated for any given node by the result for each of the surrounding elements. If there are differences the engineer can use MSC/PATRAN to smooth them out by selecting any number of averaging schemes for those nodal solutions. Conversely those averaging schemes can be entirely disabled so that the nodal differences become visually evident in the fringe plot. A poorly converged model, such as result case A1 shown in Figure 7a, indicates large element to element discontinuities in the stress fringe result. In contrast, as depicted in Figure 7b, result case A10 with averaging disabled still shows a smoothly contoured stress fringe plot.

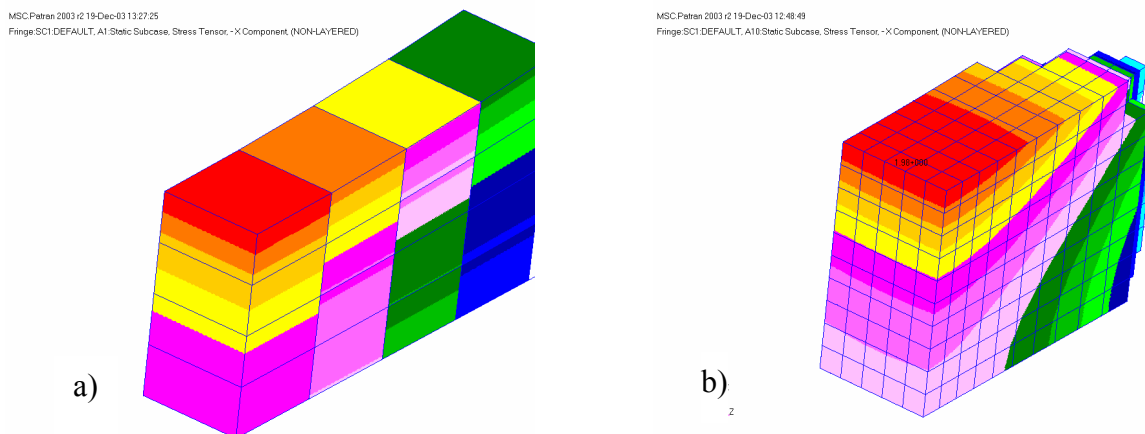


Figure 7: Example disabling the MSC/PATRAN averaging feature as a means of discerning model convergence in a) poorly converged model and a b) well converged model.

Both of these simple MSC/PATRAN techniques therefore indicate a similar confidence that the stress result is from a sufficiently converged model as that obtained by the *DoF* versus maximum stress convergence study. The σ_{MAX} from result case A10 will therefore be used to calculate K_{IN} .

Applying Equation 3 to this model we find the nominal net section stress as shown in Equation 4.

$$S_N = \frac{w_G}{w_N} \cdot lb/in^2 = \frac{1.92100 \cdot in}{1.0000 \cdot in} = 1.92100 \cdot lb/in^2 \quad (4)$$

For completeness, the calculated nominal net section stress was also verified by FEM analysis. A rectangular cross section bar with width and thickness identical to the E466 net section was modeled with a quadrilateral Hex 20 element mesh identical to the A10 result case. The net section stress from Equation 4 was applied to the positive x-axis bar end and the same symmetry boundary conditions were imposed. The stress at every net section node was identical to the calculated average stress.

The σ_{MAX} for result case A10 is found at the outside edge of the net section in the center of the thickness ($x=0$ in, $y=0.5$ in and $z=0.125$ in). This is not surprising due to the transition from plane stress at the outside free surfaces ($z=0$ & 0.25 in planes) to the plain strained condition at the thickness mid-plane. Given the relatively thin E466 specimen (as compared to the w_N however, this effect is not very dominant. In fact, the difference between the outside surface of the net section ($x=0$ in, $y=0.5$ in and $z=0$ & 0.25 in) and the center of the thickness is only 0.05%. Figure 8 shows the precise variation of stress through the thickness calculated by the FEM model at the outside edge of the net section.

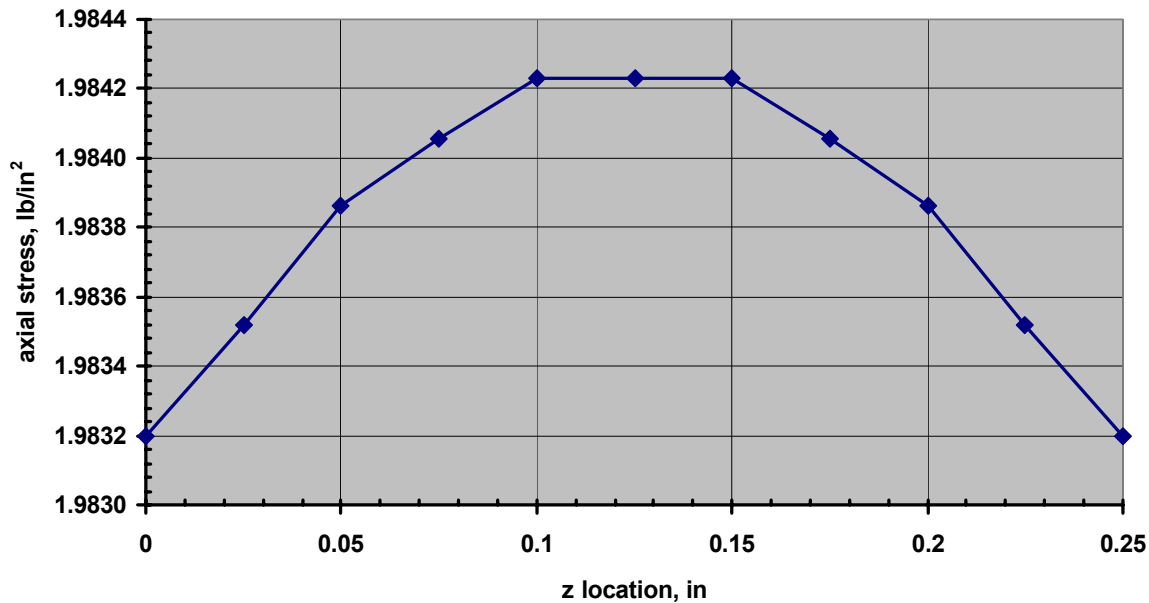


Figure 8: E466 specimen (results case A10) maximum axial stress versus through thickness (z) location at the net section outside corner ($x=0$ in, $y=0.5$ in)

The net section stress concentration factor is calculated in Equation 5.

$$K_{tN} = \frac{\sigma_{Max}}{S_N} = \frac{1.98423 \cdot psi}{1.92100 \cdot psi} = 1.03292 \quad (5)$$

Referring to Figure 2.6 in *Peterson's Stress Concentration Factors*, 2nd Edition [1], the E466 specimen's geometry results in a K_{tN} of 1.03. The minimal increase in stress at the net section of only 3% for the E466 is testament to the gentle transition from the gross section width to the net section width designed into this specimen.

2.2 ASTM E466 specimen with continuous radius between ends and net section 3/16 inch through thickness hole

In order to investigate the impact of a net section through-thickness hole upon the stress concentration, the next model included a 3/16 in hole through the center ($x=0.0$ in and $y=0.0$ in) of the net section.

Once again this specimen will be modeled as a quarter-plate with the same symmetry boundary conditions of the previous model. Given the success of the previous model with Hex 20 elements, this model would also be composed entirely of parametrically defined solids in order to be compatible with the MSC/PATRAN automatic iso-mesher. Again, these solids are easily formed by extruding a surface composed of no more than 4 sides to the specimen's thickness of 0.25 in. With the added geometric feature due to the quarter hole, this specimen's solid model was composed of five separate solids as shown in Figure 9.

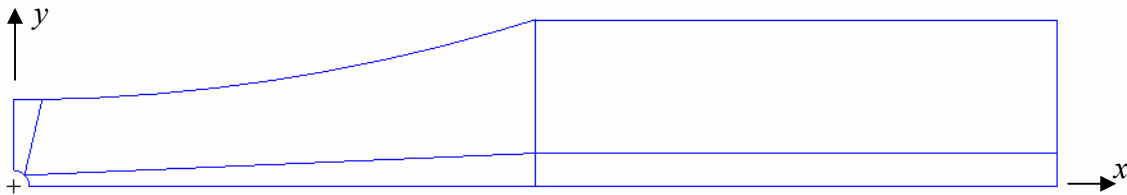


Figure 9: Solid model geometry required for MSC/PATRAN iso-meshing of E466 specimen with a net section through thickness hole.

The solids were meshed with quadrilateral Hex 20 solid elements using the MSC/PATRAN automatic mesher starting with the course default GEL (~ 0.53 in) and progressing to a GEL of 0.05 in. The net section resulting maximum (σ_{MAX}) stress versus degrees of freedom (DoF) is depicted in Figure 10.

The MSC/PATRAN mesh seeding tool was used to create a mesh density in the net section similar to that of the result case A10 from the previous model. After the seed was in place the automatic iso-mesher with default GEL was used to create a Hex 20 solid mesh with a DoF of 45,222. This result is also shown in Figure 10 as the “biased mesh” result. Again, the solution is very close to converged solutions of dramatically higher DoF . The maximum net section stress (σ_{MAX}) is 6.34418 lb/in². Also as before, the maximum stress is found in

the center of the thickness. In this case however the maximum stress is found at the “top” (x=0 in and y=0.09375 in) of the hole as viewed in Figure 9 rather than the outside extremity of the net section plan. Reviewing Equation 3, the nominal net section stress (S_N) must now take the presence of the hole for w_N in that equation. This is shown in Equation 6.

$$S_N = \frac{w_G}{w_N} \cdot lb/in^2 = \frac{1.92100 \cdot in}{(1.0000 - 0.18750) \cdot in} \cdot lb/in^2 = 2.36431 \cdot lb/in^2 \quad (6)$$

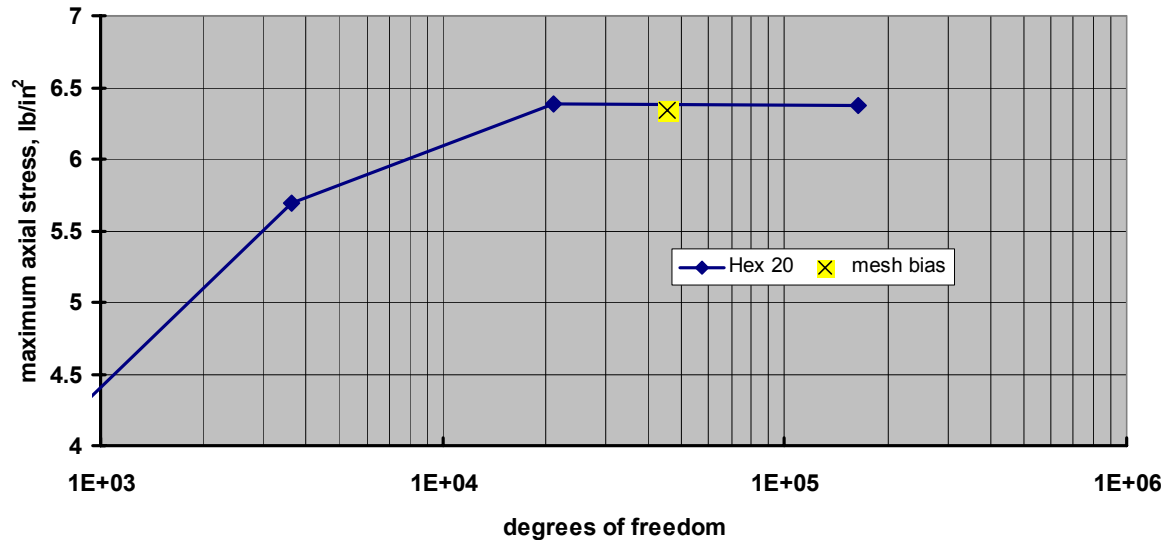


Figure 10: Degrees of freedom versus maximum net section stress for ASTM E466 specimen with 3/16 in net section through thickness hole

Using the new S_N along with the FEM model’s σ_{MAX} the net section stress concentration factor is found for this section by Equation 7.

$$K_{tN} = \frac{\sigma_{Max}}{S_N} = \frac{6.34418 \cdot psi}{2.36431 \cdot psi} = 2.68331 \quad (7)$$

Turning once again to the tabulated solutions in Peterson [1] a precise match for this configuration is not immediately forthcoming. Given that the aforementioned gentle transition from the net section to gross section width of the unaltered E466 specimen (without the through thickness hole), it is reasonable to approximate this geometry as a finite width thin element with a circular hole. This is precisely the tabulated solution found in Peterson’s Chart 4.1. Using the dimension of this specimen, namely the net section width of 1.0 in and the hole diameter of 0.1875 in the published K_{tN} is found to be 2.54267 or 5.2% less than the FEM result—the handbook K_{tN} value can be reported to 6 significant figures in this case due to the exact equation that accompanies the chart’s curve.

The apparent discrepancy is easily explained upon closer examination of the compared solutions. The published result in Peterson [1] is attributed to Howland’s [5] work in the late

1920's. Howland and others of this era calculated a host of stress distributions beginning with Timoshenko's thin panel equations. Whereas these relations were derived for thin panels, they consider only plane stress where the stress in the thickness direction is taken as negligible. These solutions are therefore independent of the thickness dimension and are consequently referred to as two-dimensional (2-D) solutions. If the panel is thick relative to its width then the plane stress assumption breaks down inside the thickness. This is due to the fact that the thickness offers restraint to interior material which leads to stress in the thickness direction under the Poisson response to the applied axial stress. If the thickness is high enough relative to the width, the restraint becomes significant enough to resist strain the thickness direction. In this case, the strain in the thickness direction is considered negligible and the material is said to be in a condition of plane strain.

Strenberg and Sadowsky [6] investigated tensile specimens of arbitrary thickness using the plane strain assumptions. For a specimen whose thickness was $3/2$ the hole radius, subjected to uniaxial tension with a Poisson's ratio of 0.3, the maximum stress was 7% less than the 2-D solution at the surface, and 3% higher at the mid-plane. Strenberg and Sadowsky go on to say the difference would become more pronounced as the ratio of thickness to hole radius increases. This observation is supported by the result presented here where the thickness of 0.25 in is $8/3$ the hole radius. Figure 11 plots the axial stress on the net section plane at the hole edge versus thickness (z) location. Also shown in this figure is the net section stress as found from the 2-D K_{tN} cataloged by Peterson [1]. The 3-D stress solutions at the outside surface and the mid-planes are 11% lower and 5% higher, respectively.

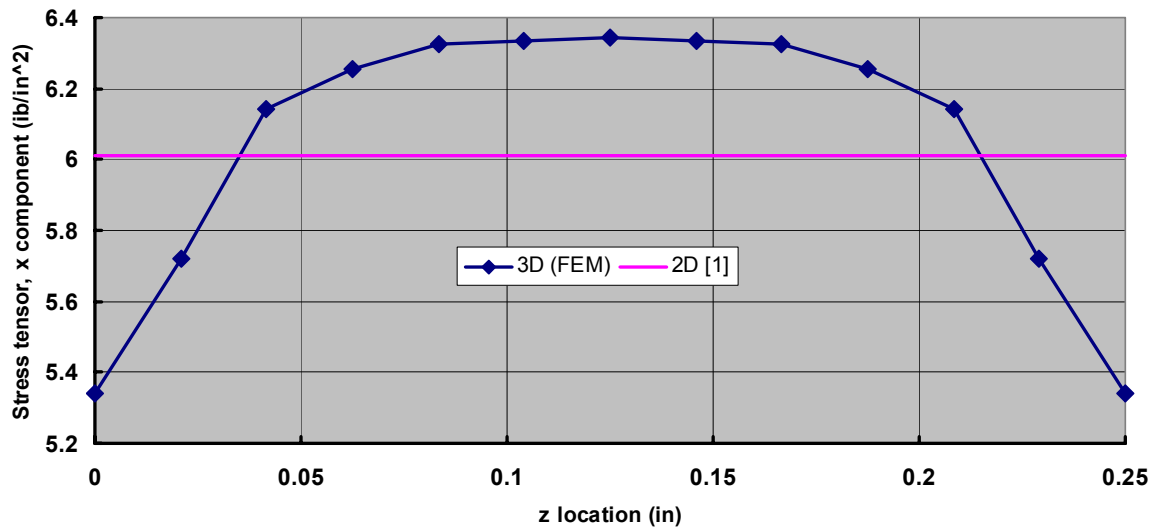


Figure 11: Comparison of FEM 3-D solution with handbook [1] 2-D solution for stress tensor x component versus through thickness (z) location at the net section top of hole ($x=0$ in, $y=0.09375$ in) of E466 specimen with $3/16$ in through thickness hole.

2.3 ASTM E466 specimen with continuous radius between ends and net section 7/16 inch through thickness hole

One additional modification to the standard E466 specimen was also explored. In this case the through thickness hole in the net section was increased to a diameter of 7/16 in. The quarter-plate model was again comprise of five separate solids (Figure 9) for the same reasons discussed with the previous model—to satisfy the requirements of MSC/PATRAN’s automatic mesh generator. Also similar to the previous model was the build up in mesh density conducted to assess solution convergence with an additional twist. The automatic mesh generator *GEL* was varied from the default setting of approximately 0.53 in to 0.05 in and the maximum value of the stress tensor x component was recorded. These results are depicted in Figure 12 as the triangles. Then the *GEL* was varied from the default down to 0.025 in only in the solids which adjoin the 7/16 in diameter quarter hole. The remaining solids were meshed using the only default settings. The default *GEL* dimension selected by MSC/PATRAN is a factor of the geometry size and element type selected during the create mesh operation. Since in the later case the two smaller solids near the hole were selected, the default *GEL* used to start that series was approximately 0.17 in. These results are also depicted in Figure 12 as the blue diamonds. As is evident from this comparison, the model solutions reaches a convergent solution at a lower *DoF* if the mesh density is increased (by progressively lower *GEL*) near the hole only rather than throughout the entire solid model. This stands to reason. Recall from Figure 3 that the greatest stress gradient occurs wherever the greatest change in geometry exist. Therefore this mesh design approach creates the greatest mesh density in the region of greatest stress gradient. Also consistent with the results of Section 2.2 and regardless of the FEM *DoF*, the maximum stress is always found on the net section plane at the top edge of the hole in the center of the plate thickness ($x=0$, $y=0.21875$ and $z=0.125$ in).

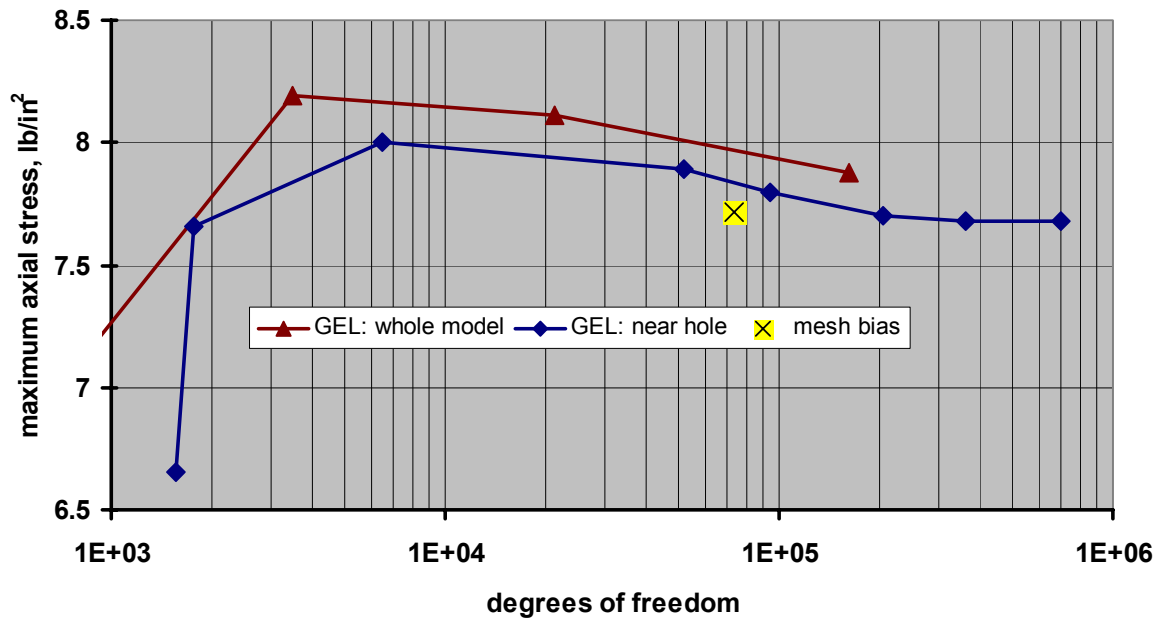


Figure 12: Degrees of freedom versus maximum net section stress for ASTM E466 specimen with 7/16 in net section through thickness hole

The mesh was once again generated using the MSC/PATRAN mesh seed tool. The seeds were applied to the edges on the net section plane ($x=0$) and around the quarter hole radius so that the mesh on those surfaces were identical to the case where the **GEL** was set at 0.025 in. The mesh was then automatically generated using default settings for all other portions of the solid model. This resulted in a MSC/PATRAN Hex 20 solid element mesh with 73,588 **DoF** whose maximum net section stress is 7.71371 lb/in^2 as shown in Figure 12 (the “mesh bias” data point.) Compare this result to the FEM solid model with $\sim 700,000$ **DoF** where the **GEL** was set to the same 0.025 in only in the solids adjacent to the hole (represented in Figure 12 by the last diamond on the blue curve.) As is obvious by this graph, both models converged to the same value with the seeded “mesh bias” model requiring an order of magnitude lower **DoF** and therefore far less computational time.

Turing to the previously discussed MSC/PATRAN *Results* tools to judge the convergence of this model one would make the same conclusion as the comparison presented in Figure 12. Figure 13 graphically summarizes the result of the two tools discussed in this work when employed on the “mesh bias” model result. In Figure 13a shows the outcome of disabling the MSC/PATRAN averaging feature for the “mesh bias” model. The continuous contour between elements qualitatively demonstrates that there is good continuity between solutions obtained in adjoining elements and is therefore considered an indication of a converged solution [4]. Figure 13b shows the maximum difference between all solutions for each node. In this case the maximum difference in the net section is shown to be $\sim 0.029 \text{ lb/in}^2$ which is less than 0.4% of the axial stress in that region—a satisfactory level of accuracy for most analyses.

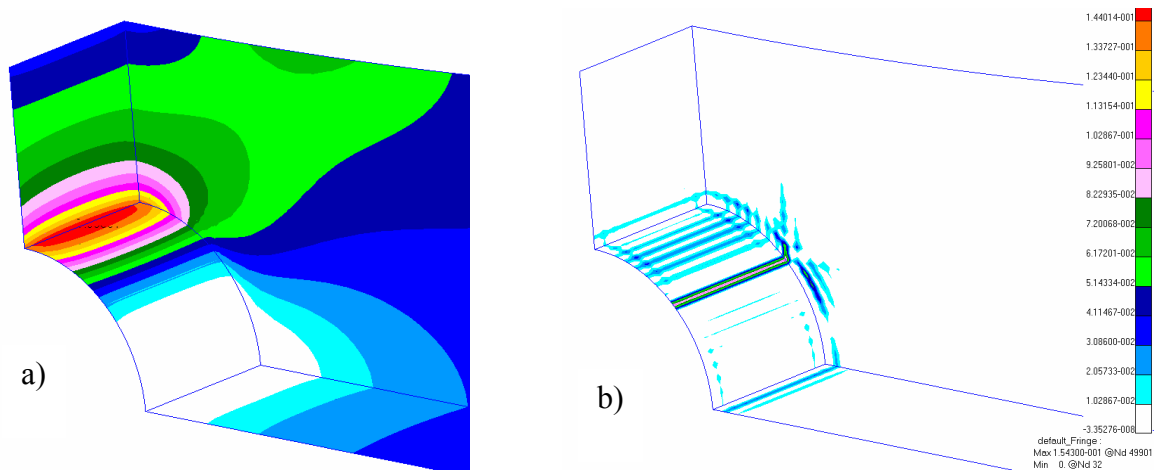


Figure 13: MSC/PATRAN contour plot of a) stress with element to element averaging disabled and b) maximum difference between all solutions for each node in the “mesh bias” model solution for E466 specimen with 7/16 in net section through thickness hole

So again, rather than using a lengthy series of FEM convergence studies, an experienced MSC/PATRAN user can take advantage of past experience to make a reasonable assumption of the initial mesh density. The user can then employ any number of convenient MSC/PATRAN *Results* tools to assess the convergence of the model and therefore the

quality of the solution. Strong caution here is that the user must fully understand the tools in order to interpret their results and their significance with respect to the model's convergence.

Finally, the “mesh bias” σ_{MAX} result is used to compute K_{tN} . Rewriting Equation 3 to account for a 7/16 in through thickness hole in the net section width, S_N is found by Equation 8.

$$S_N = \frac{w_G}{w_N} \cdot lb/in^2 = \frac{1.92100 \cdot in}{(1.0000 - 0.43750) \cdot in} \cdot lb/in^2 = 3.41511 \cdot lb/in^2 \quad (8)$$

Therefore K_{tN} is found to be approximately 2.26 as shown in Equation 9.

$$K_{tN} = \frac{\sigma_{Max}}{S_N} = \frac{7.71371 \cdot psi}{3.41511 \cdot psi} = 2.25870 \quad (9)$$

Turning to the handbook [1] for the 2-D solution for a rectangular plate with a through thickness hole for comparison one finds $K_{tN} = 2.20484$ for this configuration or 2.4% less than the FEM result. As was done in Section 3.2, the difference is also illustrated in Figure 14 by using the 2-D K_{tN} to compute the net section maximum stress.

It is worth noting here that regardless of whether the 2-D or 3-D analysis is used, the larger 7/16 in through hole results in a smaller K_{tN} than found for the 3/16 in through hole. This is completely reasonable since stress concentration factors are a measure of abruptness in the change of geometry. Recall that the ASTM E466 with no hole and an extremely gentle transition from the gross section to the net section width has only a minimal 3% stress increase due to its width change. It follows that the larger the through thickness hole radius the smoother the transition of the width dimension caused by that hole and therefore the smaller the net section stress concentration factor.

These results are also consistent with that of Strenberg and Sadowsky [6] as presented in Section 3.2. For the current specimen the thickness is 8/7 the hole radius and the 3-D solution maximum 7.4% less than the 2-D solution at the surface, and 2.4% higher at the mid-plane.

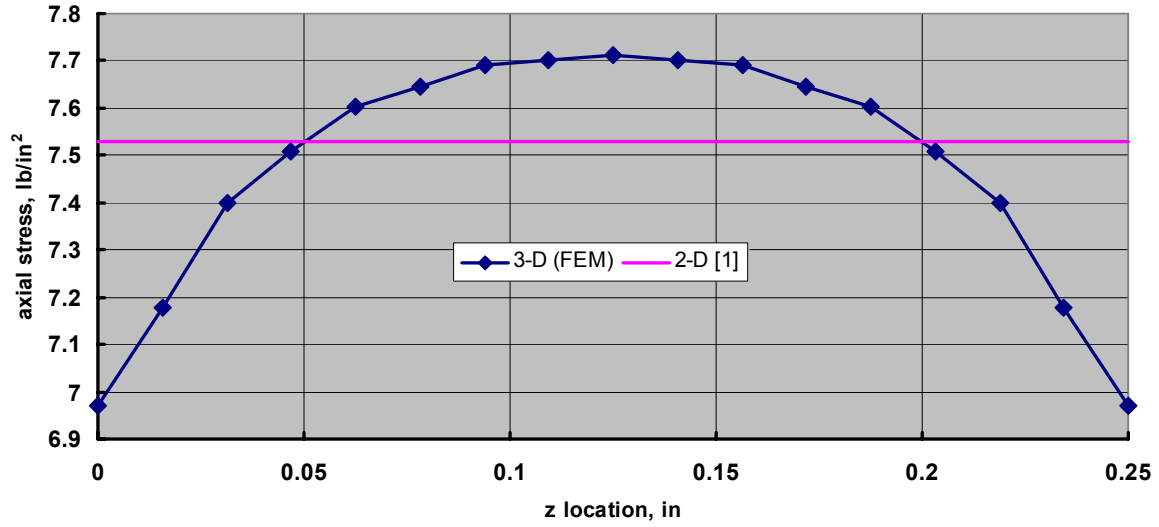


Figure 14: Comparison of FEM 3-D solution with handbook [1] 2-D solution for axial stress versus through thickness (z) location at the net section top of hole ($x=0$ in, $y=0.21875$ in) in E466 specimen with 7/16 in through thickness hole

2.4 Compact tensile test specimen for thicknesses of 0.125, 0.160 and 0.190 in.

The final solid model considered in this study was a compact tensile specimen designed to investigate the effect of exfoliation corrosion on fatigue life for a series fatigue effect from exfoliation studies in the CASTLE Research Center. In contrast to the ASTM 466, this specimen features a more abrupt transition from the gross section to the net section width. Figure 15 is the plan view of this design.

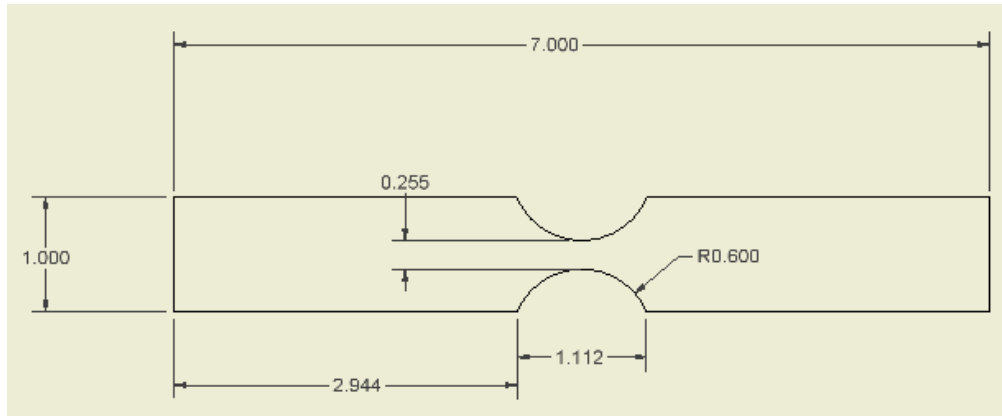


Figure 15: Plan view of compact test specimen used in CASTLE Research Center fatigue effect from exfoliation studies

To be consistent with the previous three models this shape was modeled as a quarter plate in MSC/PATRAN with symmetry displacement constraints boundary conditions were imposed along the entire xz -plane at $y=0$ and yz -plane at $x=0$. As viewed in Figure 16, the 1 lb/in^2 gross section stress (S_G) was applied to the entire yz -plane at $x=3.5 \text{ in}$. In this figure the origin is at the lower left corner.

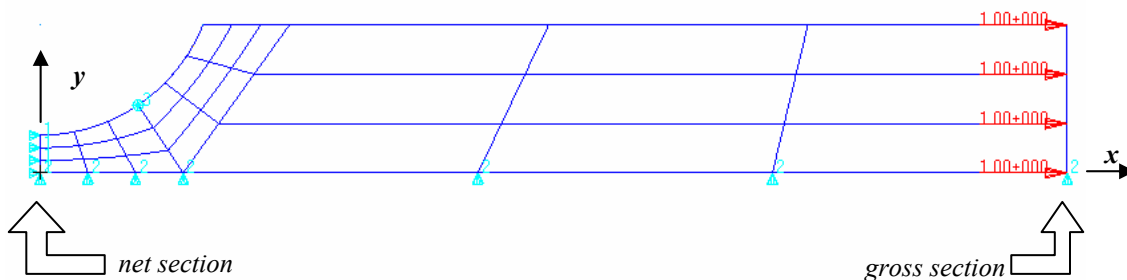


Figure 16: Compact tensile specimen quarter plate model used for the analysis showing boundary conditions, loads and solid geometry. Net and gross section planes are noted.

In order to demonstrate how an experienced MSC/PATRAN user might approach this sort of problem, the element mesh was generated directly using the experience gained during the creation of the previous three convergent models. The MSC/PATRAN *Results* tools would then be used to assess the quality of these models.

Once again Hex 20 solid elements were chosen for the FEM model. As with previous results, maximum stress is expected on the inside of the hole on the net section plane ($x=0$)

and $y=0.1275$ in). As a starting place, the MSC/PATRAN mesh seed tool was used to define an element density through the thickness and on the net section plane similar to the convergent E466 FEM models. Specifically, the 0.125 in thick compact specimen would have 5 Hex 20 elements across its thickness. The radius edge was also seeded such that the elements on the hole edge would have nearly the same edge length on all edges. Lastly the mesh seed was used to create a smooth transition to larger element edge dimensions (up to 0.3 in) in the gross section side of the solid. This mesh seeding produced a FEM solid model with 38,894 *DoF*.

The solution of this model yields a maximum axial stress of 4.45060 lb/in^2 on the outside of net section plane at the thickness mid-plane ($x=0$, $y=0.1275$ and $z=0.0625$ in). Exploring the quality of this solution using the MSC/PATRAN *Results* tools the fringe plots of Figure 17 were generated.

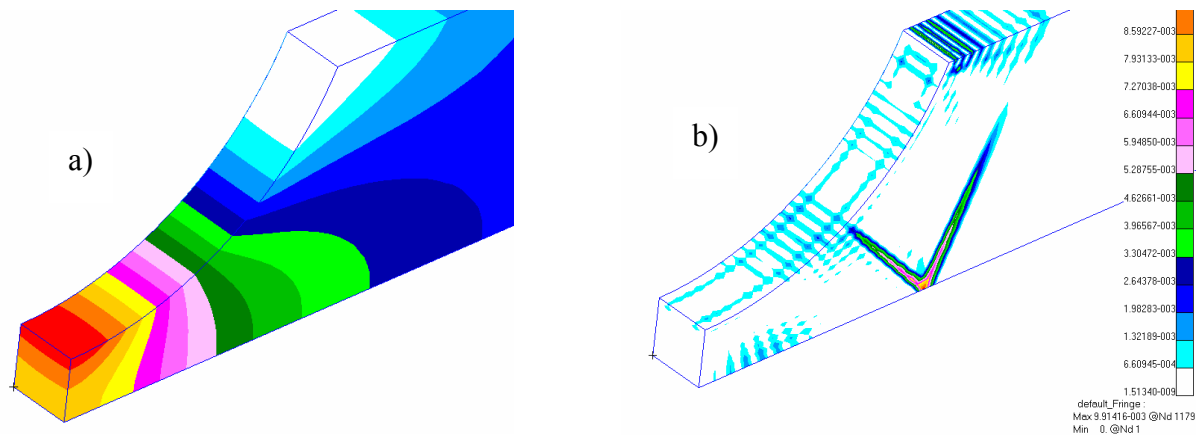


Figure 17: MSC/PATRAN contour plot of a) stress with element to element averaging disabled and b) maximum difference between all solutions for each node in the 0.125 in thick compact test specimen model

Recall the use of the MSC/PATRAN averaging tool to qualitatively discern model convergence as presented in Figure 7. The smooth contours of the axial stress plot in Figure 17a gives confidence in these results without timely convergence studies. Further confidence is afforded by quantitatively exploring the differences in individual nodal solutions derived from the adjoining element solutions. Recall that these differences are likened to the error of the analytical result. Interrogating the maximum node difference result depicted in Figure 17b we find that the maximum nodal difference in the net section plane ($x=0$) is less 0.00132 lb/in^2 or less than 0.03% of the maximum stress in that plane. Accepting this level of accuracy in the analytical result for the maximum stress of this model, the 3-D K_{IN} can now be calculated.

Using Equation 3, S_N for the compact tensile specimen is found by Equation 10.

$$S_N = \frac{w_G}{w_N} \cdot \text{lb/in}^2 = \frac{1.0 \cdot \text{in}}{0.2550 \cdot \text{in}} \cdot \text{lb/in}^2 = 3.92157 \cdot \text{lb/in}^2 \quad (10)$$

And the corresponding K_{tN} is given by Equation 11.

$$K_{tN} = \frac{\sigma_{Max}}{S_N} = \frac{4.45060 \cdot lb/in^2}{3.92157 \cdot lb/in^2} = 1.13490 \quad (11)$$

The published data [1] for tensile specimens of this configuration gives $K_{tN} = 1.13$. Again, the handbook K_{tN} is for a 2-D solution under a plane stress assumption. While the influence of thickness and the corresponding transition to plane strain near the mid-plane is present in this FEM solution it is minimal. The stress on the surface at the same x-y plane location is only 0.8% less for this model's solution.

Since the 2-D solution is known to be independent of thickness, the effect of thickness upon the 3-D FEM solution was explored by modeling the same specimen with a thickness 0.160 in. Symmetry boundary conditions and applied gross section stress is the same as for the 0.125 in solid model. The same elements and the same mesh seed is used for this 0.160 in thick model with the exception of the thickness direction itself. To keep the same approximate 0.025 in element edge dimension while accounting for the increased thickness, the mesh seed is set to generate 7 Hex 20 elements through the thickness. This mesh seed with MSC/PATRAN defaults used for the remainder of the model creates a model with 49,738 *DoF*. For this model the maximum axial stress of 4.45842 lb/in² occurs at the same mid-plane thickness location on the outside of the net section (x=0, y=0.1265 and z=0.80 in). The model solution is evaluated both qualitatively and quantitatively using the MSC/PATRAN *Results* tools presented in Figure 17. In this case the quantitative assessment of node solution difference (Figure 17b) yields a worse case error in the net section of less than 0.03% of the net section axial stress result. The slightly thicker model's solution yields a correspondingly slightly higher thickness effect in the 3-D FEM stress result. In this case the surface stress is 1.2% lower than the mid-plane value.

Exploring the thickness impact one step further, the whole process is repeated for a solid model thickness of 0.190 in. Now the thickness is seeded to produce a mesh with 8 Hex 20 elements through the thickness resulting in a model with 56,160 *DoF*. The maximum axial stress in the net section is now 4.46685 lb/in² and the surface stress is 1.7% lower than the mid-plane value. Qualitative and quantitative assessment of the 0.190 in thick solid model remains unchanged.

The K_{tN} values for the 0.160 in and 0.190 in thick FEM models are 1.13690 and 1.13905, respectively. Axial stress at the outside edge of the net section (x=0 and y=0.1275 in) as function of thickness location for all three thicknesses is summarized in Figure 18. For easy comparability the thickness location is expressed as a fraction of total thickness. The thickness independent stress obtained from the 2-D plane stress handbook solution is included as a reference.

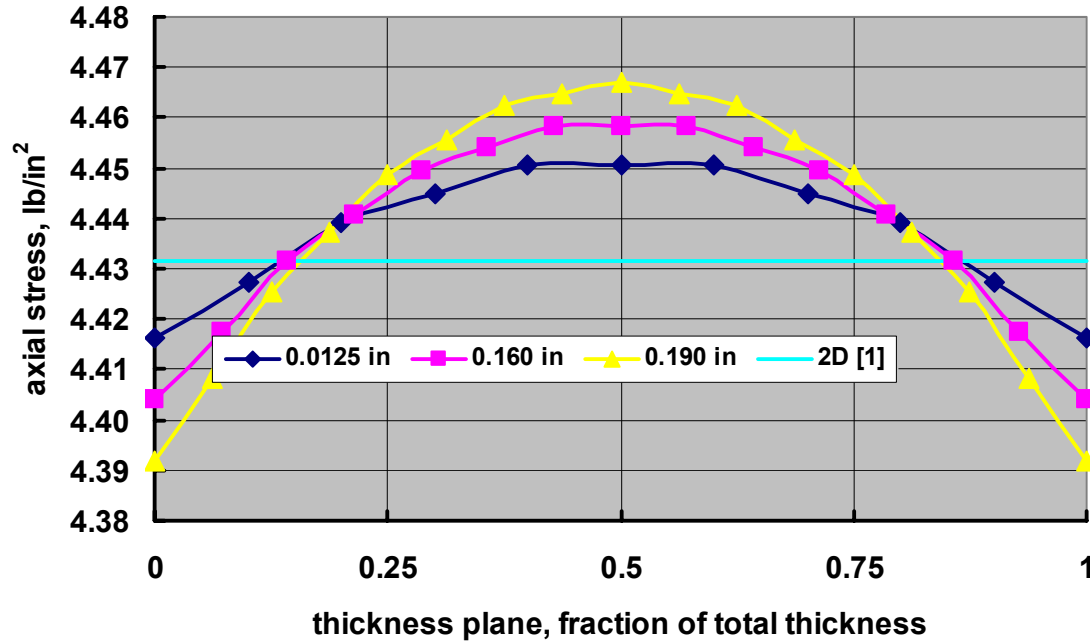


Figure 18: Axial stress from 3-D FEM solution versus thickness plane for three thicknesses modeled of the compact tensile test specimen. Handbook [1] 2-D solution is also shown

3. Discussion

Table 2 summarized the results of the present work. The through thickness variation of stress at the maximum stress net section x-y planer location is represented by the increase from the surface value to the mid-plane value. Next the Table compares the 3-D FEM K_{tN} solution for each specimen modeled with the 2-D K_{tN} from Peterson [1]. The percentage the 3-D value is greater than the 2-D value (if any) is also noted.

Table 2: Summary of FEM 3-D K_{tN} results compared with 2-D handbook [1] K_{tN}

Specimen	Stress increase from surface to mid-plane	3-D K_{tN} (FEM)	2-D K_{tN} [Ref 1]	$1 - \frac{K_{tN-3D}}{K_{tN-2D}}$
ASTM E466 specimen	0.05 %	1.033	1.030	<1 %
ASTM E466 specimen with 3/16 hole	18.7 %	2.683	2.543	5.5 %
ASTM E466 specimen with 7/16 hole	10.7 %	2.259	2.205	2.4 %
Compact tensile specimen, 0.125 in thick	0.78 %	1.135	1.130	<1 %
Compact tensile specimen, 0.160 in thick	1.24 %	1.137	1.130	<1 %
Compact tensile specimen, 0.190 in thick	1.71 %	1.139	1.130	<1 %

As illustrated in Table 2, the 2-D stress concentrations values are not in *precise* agreement with the 3-D analysis. However, since in four of the six configurations modeled this difference is less than 1%, the 2-D solutions are adequate for many types of structural analysis. Some might even argue that the worst error, 5.5%, is not worth the additional burden of a FEM analysis as the 2-D solutions are generally easily available by a simple table lookup or application of the appropriate equation.

The 3-D solution differs because it takes into account the fact that the stress in a tensile specimen is not constant through the thickness. The 2-D stress concentration factors commonly found in handbooks are developed using elasticity relations under a plane stress assumption. This assumption, while very good for thin members, is not entirely valid. Thicker specimens and those with sharp width transitions relative to the thickness serve to decrease the validity of the plane stress assumption [7]. In these cases the mid-plane in the specimen's thickness tends to be more accurately represented by elasticity relations developed using plane-strain assumption. This observation is evidenced in the present work by the two specimens which not only transition from a gross section width to a net section width but also include a through thickness hole in the net section. It should stand to reason that the larger the deviation between the surface stress and the mid-plane stress, the larger the deviation between the 3-D solution and the 2-D solution.

Using the through thickness stress variation as a guide to when a FEM analysis is necessary to obtain accurate K_{tN} values is unfortunately not very helpful. This is of course because the FEM work is necessary to make this determination in the first place. The engineer can however perform an analysis on a sample in a particular category of specimen configurations to ascertain to what extent the 2-D solutions may be relied upon. This judgment of course must also be tempered by the character of the analysis involved. For example, rough sizing of structural components would most likely be well served by K_{tN} values that are "only" good to ~5%. At the same time, better crack growth predictions result from a more accurate picture of through thickness stress.

All FEM models used for the analysis presented here were assessed for solution validity by determining model convergence. Convergence was determined by comparing the solution of models with increasingly fine meshes and therefore increasing large *DoF*. When the model solution became invariant despite increasing the *DoF*, the model was considered convergent and the solution could be trusted for the analysis at hand. This technique required a large number of NASTRAN runs of the same solid geometry with the increasing *DoF*. Depending on the size of the model such a technique can become prohibitively expensive in terms of both computer time and FEM engineer time. The alternative presented was to use past FEM experience for an initial judgment of mesh size in a particular geometry. The MSC/PATRAN *Elements* mesh seed tool quickly turns the judgment into a solid mesh ready for NASTRAN analysis. Once a solution is obtained, the MSC/PATRAN post processing *Results* tools can be used to both qualitatively and quantitatively assess the validity of the model. These techniques quickly compare the consistency of the solution from element to element across the entire solid model. An experienced user can alter the mesh as necessary to obtain the required level of accuracy in the solution. In the present work, both techniques were used and compared to each other. The comparison demonstrated that both techniques

are equally valid. The key to trusting the MSC/PATRAN *Results* tools is training and experience of the user. Depending on the size of the model this technique may in fact be the best choice. A good example would be in extremely large and/or detailed models where lengthy convergence studies and the associated mesh variations may not be practical.

4. Conclusion and Recommendations

Stress risers in structural components are a necessary fact of design. The stress concentration factors used to describe the magnitude of these risers can be obtained from published charts, tables and equations which match the geometry of the stress riser. Published factors are typically found from a 2-D elasticity analysis. Alternatively, these factors can also be obtained from 3-D solid FEM models. This work showed some examples of stress risers in typical tensile test specimens and the stress concentration resulting from both the 2-D handbook data and a 3-D solid model FEM analysis. The engineer should carefully consider the accuracy required in the analysis along with the particular stress riser involved when deciding whether to use the 2-D handbook value or opt for a 3-D analysis.

If a 3-D FEM analysis is chosen, MSC/PATRAN offers several pre- and post- processing tools to simplify an MSC/NASTRAN analysis. These tools help an experienced engineer assess the validity of a particular FEM solution without what may be a prohibitively time consuming convergence study. This is particularly with multi-element models and those requiring the use of extensive contact regions where element choice is limited and multiple variations of the mesh is impractical. An FEM engineer who is well trained in the application of the MSC/PATRAN post processing features can obtain a valid solution with confidence. The best recommendation here is that once the engineer is trained in the use of these tools that experience is gained by their application to increasingly complex models.

5. References

1. Pilkey, W. D., *Peterson's Stress Concentration Factors*, 2nd Edition, John Wiley and Sons, Inc., New York, NY, pp. 86, 256, 1997.
2. Young, W. C. and Budynas, R. G., *Roark's Formulas for Stress and Strain*, 7th Ed., McGraw-Hill, New York, NY, 2002.
3. *Standard Practice for Conducting force Controlled Constant Amplitude Axial Fatigue Tests of Metallic Materials*, ASTM Standard E466, ASTM International, West Conshohocken, PA, 2002.
4. *PAT301 Introduction to MSC.PATRAN Course Notes*, MSC.Software Corporation, Santa Ana, CA, 2002.
5. Howland, R. C. J., "On the Stresses in the Neighborhood of a Circular Hole in a Strip under Tension," *Philosophical Transactions Of the Royal Society (London) A*, Vol 229, pp. 67, 1929-30.
6. Sternberg, E. and Sadowsky, M. A., "Three-Dimensional Solutions for the Stress Concentration Around a Circular Hole in a Plate of Arbitrary Thickness," *Transactions of ASME, Applied Mechanics Section*, Vol. 71, pp. 27, 1949.
7. Niu, C. Y. M., *Airframe Structural Design*, Conmilit Press, Ltd., Hong Kong, pp. 97, 561-563, 1991.